

Anomalous Hall effect in ferromagnetic $LaCo_2As_2$ and ferrimagnetic $NdCo_2As_2$

Yu-Qing Huang(黄雨晴), Peng-Yu Zheng(郑鹏宇), Rui Liu(刘瑞), Xi-Tong Xu(许锡童), Zi-Yang Wu(吴紫阳), Chao Dong(董超), Jun-Feng Wang(王俊峰), Zhi-Ping Yin(殷志平), and Shuang Jia(贾爽)
Citation: Chin. Phys. B, 2023, 32 (**10**): 107502. DOI: 10.1088/1674-1056/acd925
Journal homepage: http://cpb.iphy.ac.cn; http://iopscience.iop.org/cpb

What follows is a list of articles you may be interested in

Magnetic and electronic properties of bulk and two-dimensional $FeBi_2Te_4$: A first-principles study

Qianqian Wang(王倩倩), Jianzhou Zhao(赵建洲), Weikang Wu(吴维康), Yinning Zhou(周胤宁), Qile Li, Mark T. Edmonds, and Shengyuan A. Yang(杨声远)
Chin. Phys. B, 2023, 32 (**8**): 087506. DOI: 10.1088/1674-1056/acd522

Topological magnetotransport and electrical switching of sputtered antiferromagnetic $Ir_{20}Mn_{80}$

Danrong Xiong(熊丹荣), Yuhao Jiang(蒋宇昊), Daoqian Zhu(朱道乾), Ao Du(杜奥), Zongxia Guo(郭宗夏), Shiyang Lu(卢世阳), Chunxu Wang(王春旭), Qingtao Xia(夏清涛), Dapeng Zhu(朱大鹏), and Weisheng Zhao(赵巍胜)
Chin. Phys. B, 2023, 32 (**5**): 057501. DOI: 10.1088/1674-1056/acb9ec

Enhancement of spin-orbit torque efficiency by tailoring interfacial spin-orbit coupling in Pt-based magnetic multilayers

Wenqiang Wang(王文强), Gengkuan Zhu(朱耿宽), Kaiyuan Zhou(周恺元), Xiang Zhan(战翔), Zui Tao(陶醉), Qingwei Fu(付清为), Like Liang(梁力克), Zishuang Li(李子爽), Lina Chen(陈丽娜), Chunjie Yan(晏春杰), Haotian Li(李浩天), Tiejun Zhou(周铁军), and Ronghua Liu(刘荣华)
Chin. Phys. B, 2022, 31 (**9**): 097504. DOI: 10.1088/1674-1056/ac76aa

Magnetic characterization of a thin $Co_2MnSi/L1_0$–MnGa synthetic antiferromagnetic bilayer prepared by MBE

Shan Li(黎姗), Jun Lu(鲁军)†, Si-Wei Mao(毛思玮), Da-Hai Wei(魏大海), and Jian-Hua Zhao(赵建华)
Chin. Phys. B, 2020, 29 (**10**): 107501. DOI: 10.1088/1674-1056/ab99ac

Anomalous Hall effect in ferromagnetic Weyl semimetal candidate $Zr_{1-x}V_xCo_{1.6}Sn$

Guangqiang Wang(王光强), Zhanghao Sun(孙彰昊), Xinyu Si(司鑫宇), Shuang Jia(贾爽)
Chin. Phys. B, 2020, 29 (**7**): 077503. DOI: 10.1088/1674-1056/ab8da8

Anomalous Hall effect in ferromagnetic $LaCo_2As_2$ and ferrimagnetic $NdCo_2As_2$

Yu-Qing Huang(黄雨晴)[1,2], Peng-Yu Zheng(郑鹏宇)[3], Rui Liu(刘瑞)[3], Xi-Tong Xu(许锡童)[1], Zi-Yang Wu(吴紫阳)[4], Chao Dong(董超)[4], Jun-Feng Wang(王俊峰)[4], Zhi-Ping Yin(殷志平)[3], and Shuang Jia(贾爽)[1,2,5,†]

[1] *International Center for Quantum Materials, School of Physics, Peking University, Beijing* 100081, *China*
[2] *Foshan Xianhu Laboratory of the Advanced Energy Science and Technology Guangdong Laboratory, Xianhu Hydrogen Valley, Foshan* 528200, *China*
[3] *Department of Physics and Center for Advanced Quantum Studies, Beijing Normal University, Beijing* 100875, *China*
[4] *Wuhan National High Magnetic Field Center and School of Physics, Huazhong University of Science and Technology, Wuhan* 430074, *China*
[5] *Kunshan Innovation Institute of Nanjing University, Kunshan* 215347, *China*

(Received 14 April 2023; revised manuscript received 26 May 2023; accepted manuscript online 26 May 2023)

We conducted a comparative study of the magnetic and transport properties of single-crystalline $LaCo_2As_2$ and $NdCo_2As_2$. $LaCo_2As_2$ is a soft metallic ferromagnet which exhibits purely intrinsic anomalous Hall effect (AHE) due to Co-3d electrons. With Nd-4f electronic magnetism, ferrimagnetic $NdCo_2As_2$ manifests pronounced sign reversal and multiple hysteresis loops in temperature- and field-dependent magnetization, Hall resistivity, and magnetoresistance, due to complicated magnetic structural changes. We reveal that the AHE for $NdCo_2As_2$ is stemming from the Co sub-lattice and deduce its phase diagram which includes magnetic compensation and two meta-magnetic phase transitions. The sensitivity of the Hall effect on the details of the magnetic structures in ferrimagnetic $NdCo_2As_2$ provides a unique opportunity to explore the magnetic interaction between 4f and 3d electrons and its impact on the electronic structure.

Keywords: anomalous Hall effect, ferrimagnetism, magnetic compensation, meta-magnetic transitions

PACS: 75.47.–m, 75.50.Gg, 75.30.Kz **DOI:** 10.1088/1674-1056/acd925

1. Introduction

The anomalous Hall effect (AHE), which generally occurs in the conductive ferromagnetic (FM) materials, describes the phenomenon that an electrical current flows perpendicular to an electrical bias due to a non-zero internal magnetization.[1] There has been a chronic debate on whether the AHE is steming from an intrinsic electronic band effect of an unperturbed crystal or from an extrinsic magnetic impurity scattering.[2–5] A remarkable step forward of the theory is the connection between the intrinsic AHE and Berry curvature field in the relativistic band structure of FM materials.[1,6] The development of Berry phase physics breaks the paradigm of the scaling of the AHE with the strength of magnetization. The AHE has been experimentally observed in various antiferromagnetic (AFM) compounds with small or even null net magnetization (M_S).[7–9]

Ferrimagnetism (FIM) is a type of long-range magnetic ordering which can be regarded as an AFM with two unequal magnetic sub-lattices.[10] Because of the anti-parallel coupling of the sub-lattice moments, an FIM material generally has small M_S which takes complicated dependence on the temperature and external magnetic field.[11,12] As the magnitude and the interaction strength of the sub-lattice moments change at finite temperature, the direction of M_S can reverse when cooling an FIM material from its critical temperature to zero temperature. The most well-known FIM materials are rare-earth–transition-metal (R-TM) alloys in which the R and TM atoms are randomly distributed. Their magnetic moments cancel each other out at the magnetic compensation temperature (T_{comp}) and the M_S converges to zero.[13,14] A wide range of fast magnetic dynamic phenomena, including optical switching,[15] current-induced magnetization switching,[16,17] and domain wall motion[18] were observed near T_{comp} in R-TM alloys, which render them as promising candidates for future spintronic devices with higher speed and density.[4,9] In finite external field, the R-TM alloy can undergo a series of meta-magnetic transitions (MMTs), from an FIM in zero field to a spin-flop transition at the critical field of H_{sf} and finally to a saturated state in which the magnetic moments of R and TM align collinearly.[20,21] The AHE is a reliable signature for detecting the magnetic compensation and the MMTs in the R-TM FIM thin films.[22–25]

Unlike in R-TM alloys, the AHE in FIM compounds remains virtually unexplored until recently. First principle calculations predict a nontrivial intrinsic AHE in compensated Heusler ferrimagnets.[26,27] A large intrinsic AHE in FIM RMn_6Sn_6 is stemming from the strong Berry curvature field of Chern-gapped Dirac fermion in Mn-based kagome lattice.[28,29] Here we focus on the AHE and magnetotransport properties of FIM $NdCo_2As_2$ and FM $LaCo_2As_2$. Unlike

†Corresponding author. E-mail: gwljiashuang@pku.edu.cn
© 2023 Chinese Physical Society and IOP Publishing Ltd

RMn_6Sn_6, in which the magnetization of Mn sub-lattice prevails that of R, the magnetizations of Co and Nd sub-lattices are comparable in $NdCo_2As_2$. Since the Co and R atoms are periodically distributed in the crystal structure, the magnetic structure of $NdCo_2As_2$ is much more complicated than that of R-TM alloys. In this work, we find that the AHE is a sensitive signature for identifying the magnetic structure change in this FIM compound.

Crystallized in a $ThCr_2Si_2$-type structure, RCo_2As_2 is formed by stacking covalently bonded Co_2As_2 layers with R atoms[30] (Fig. 1(a)). The magnetic properties of cobalt-based $ThCr_2Si_2$-type compounds have delicate relationship with the electron count and crystal structure.[31–33] When the R atom is lanthanum which has no 4f electron, $LaCo_2As_2$ shows an FM ground state with a Curie temperature of T_C = 178 K and the saturated magnetization M_{sat} being 0.59 μ_B/Co atom.[34–37] $CeCo_2As_2$ is an FM Kondo lattice which exhibits a significantly enhanced intrinsic AHE.[38] When the R atom is neodymium which bears well-defined local moment of the $4f^3$ electronic configuration, $NdCo_2As_2$ manifests an FIM state in which the magnetic moments of the Co sublattice are anti-parallel to that of the Nd sub-lattice.[33–35] Previous magnetization measurement on the polycrystalline sample of $NdCo_2As_2$ demonstrated signatures of magnetic compensation and MMTs.[34] However, due to the lack of electrical transport and magnetic properties for the single-crystalline samples, the ground state and the nature of the MMTs in $NdCo_2As_2$ have not been fully understood.

In order to better understand the AHE in $NdCo_2As_2$, we comparably investigated the magnetic and transport properties of single-crystalline $LaCo_2As_2$. As a non-4f-electron counterpart, the metallic FM $LaCo_2As_2$ has purely intrinsic AHE originating from the Berry curvature field, which is consistent with the first principle calculation. In contrast, FIM $NdCo_2As_2$ displays pronounced sign reversal and multiple hysteresis loops in temperature- and field-dependent magnetization, Hall resistivity (ρ_{yx}), and magnetoresistance (MR = $(\rho(H)-\rho(0))/\rho(0)$). Realizing the contribution from the Co sub-lattice dominates in the AHE for $NdCo_2As_2$, we deduced a complicated phase diagram which contains magnetic compensation and multiple MMTs. Our results demonstrate the extreme sensitivity of the Hall effect on the details of the magnetic structures in an FIM compound.

2. Method

Single crystals of RCo_2As_2 were grown from Bi flux as reported in Refs. [34–36,39]. However, we found that the remnant bismuth in the sample conducts electric current in the electrical measurement and brings serious misreading of its transport properties. To overcome this issue, we used a self-flux solution-growth technique to grow single crystals of $LaCo_2As_2$ and $NdCo_2As_2$. Precursor CoAs was synthesized by reacting cobalt powder (99.9%, Alfa Aesar) and As lumps (99.9%) in a sealed fused silica ampule at 1170 K for 12 hours. Then lanthanum ingots (99.9%, Alfa Aesar), neodymium ingots (99.9%, Alfa Aesar) and CoAs lumps were packed in an alumina crucible with a molar ratio of 1:3. The crucible was then loaded into a fused silica ampule which was sealed with argon gas at 0.1 atm (1 atm = 1.01325×10^5 Pa). The ampule was heated to 1423 K in 10 h and held at this temperature for a week. Several plate-like single crystals with dimensions approximate 0.4 mm×0.5 mm×0.1 mm were separated after centrifugation at 1423 K. The crystal structure was confirmed by powder x-ray diffraction (Cu K_α) measurements at room temperature in a Rigaku MiniFlex600 diffractometer.

Electrical transport measurements for polished single crystals were carried out in a quantum design physical property measurement system (PPMS-9). The standard four-point method was adopted and silver paste was used as the contacts. The longitudinal resistivity and Hall resistivity measurements were conducted with fields normal to and currents within the *ab* plane. The size of samples was measured using a reading microscope to calculate the electrical resistivities, and the dimension error is estimated at about 10%. A quantum design magnetic property measurement system (MPMS-3) was used to perform the magnetization measurement with the applied field direction being along the crystallographic *c* axis on the samples.

We performed density functional theory (DFT) calculations to compute the electronic structure of $LaCo_2As_2$ in the FM state by using the Vienna *ab initio* simulation package (VASP).[1] We used the experimental lattice parameters for $LaCo_2As_2$.[39] The projected augmented wave method and the generalized gradient approximation (GGA) of Perdew–Burke–Ernzerhof (PBE) were chosen. The plane-wave-basis cut-off energy was set to be 600 eV. As for the topological property, the Berry curvature and anomalous Hall conductivity (AHC) were calculated with the tight-binding (TB) method with Wannier90[41] and WannierTools softwares.[42]

In order to capture the electronic correlation effect, we first performed density functional theory plus dynamical mean-field theory (DFT + DMFT) calculations[43,44] to compute the electronic structure of $LaCo_2As_2$ in the FM states. The DFT part was calculated by the linearized augmented plane-wave method as implemented in WIEN2k.[45] The PBE exchange–correlation functional was used. We treated Co-3d correlated and Hubbard U = 5.0 eV, Hund's coupling J = 0.8 eV were used, in consistent with the previous calculations.[46] We chose the "exact" double-counting scheme to solve the double counting problem.[47] The impurity problem in DFT + DMFT was solved by using the continuous time quantum Monte Carlo method at T = 100 K.[48,49]

Then, we renormalized the TB parameters obtained from the DFT calculations to fit the DFT+DMFT calculated band structure around the Fermi level and then shifted the Fermi level before plotting the band structure and computing the topological property.

3. Results

As shown in Fig. 1, the magnetic properties of the $LaCo_2As_2$ crystals grown from CoAs flux are identical to those from Bi flux.[34–36,39] Temperature-dependent magnetization ($M(T)$) in an applied field $\mu_0 H = 0.1$ T shows an FM state with an easy-c-axis and T_C of around 170 K. The soft FM state is verified by isothermals of magnetization below T_C (Fig. 1(c)), which shows an M_{sat} being 1.1 μ_B per formula unit (f.u.) at 2 K. Temperature dependence of resistivity ($\rho(T)$) has a profile of a metal with a significant slope change at T_C, most likely due to loss of spin-disorder scattering in the FM state.

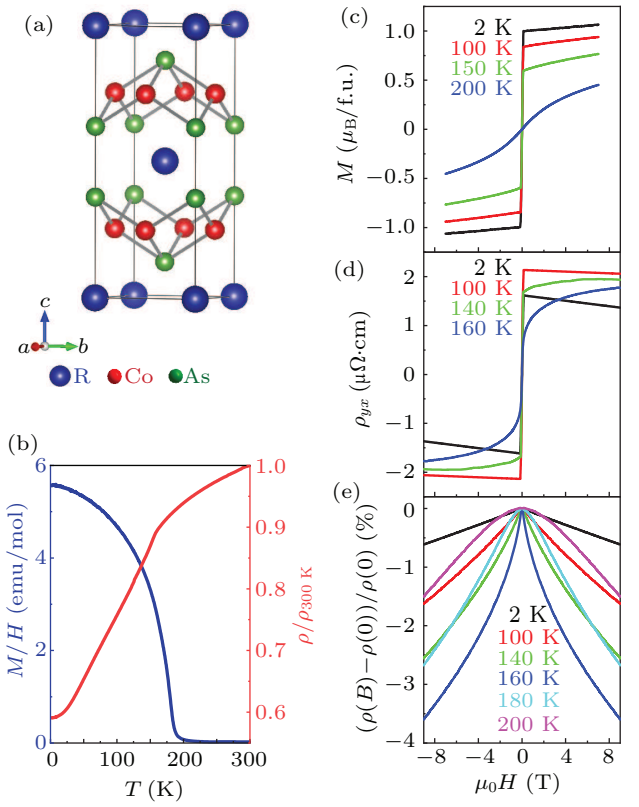


Fig. 1. Magnetic properties of $LaCo_2As_2$. (a) Unit cell of RCo_2As_2. (b) Temperature dependence of the magnetization (blue) in an external magnetic field of 0.1 T along the crystallographic c axis, and normalized zero-field longitudinal electrical resistivity $\rho/\rho_{300\ K}$ (red). (c)–(e) Magnetization, Hall resistivity, and MR with respect to the applied field along the direction of c axis at representative temperatures, respectively.

Isothermals of $\rho_{yx}(H)$ and MR with respect to the applied field are shown in Figs. 1(d) and 1(e), respectively. Negative MR is commonly observed in FM metals due to suppression of the spin-disorder scattering by an external field. The $\rho_{yx}(H)$ approximately follows the magnetic isothermals, revealing a pronounced spontaneous AHE. Empirically, ρ_{yx} of an FM material comprises two terms[1]

$$\rho_{yx} = \rho_{yx}^{O}(B) + \rho_{yx}^{AH}(M) = R_0 B + \mu_0 R_S M, \tag{1}$$

where ρ_{yx}^{O} represents the ordinary Hall resistivity, ρ_{yx}^{AH} the anomalous Hall resistivity, R_0 the ordinary and R_S the anomalous Hall coefficient. Fitting the data at 2 K, we obtained R_0 being -2.8×10^{-4} cm^3/C and R_S being 4.4×10^{-5} cm^3/C, leading to $n = -2.30 \times 10^{22}$ cm^{-3}, a typical electron density for an n-type metal.

Next, we demonstrate the magnetic and electrical transport properties of the single crystals of $NdCo_2As_2$. Its $M(T)$ has a typical profile of an FIM which has T_C around 90 K and T_{comp} around 10 K (Fig. 2(a)). Because the Co sub-lattice orders ferromagnetically along c axis at first, M has an abrupt increase when temperature is below T_C. The moments of Nd atoms are gradually ordered under the influence of the internal field induced by the Co sub-lattice. Because the Co and Nd magnetic moments intend to align in anti-parallel, M_S starts to drop below 33 K. The contributions from the two sub-lattices become nearly equal at about 10 K which is the T_{comp} for $NdCo_2As_2$, very close to the literature report.[34,35] At lower temperature the $M(T)$ abruptly increases.

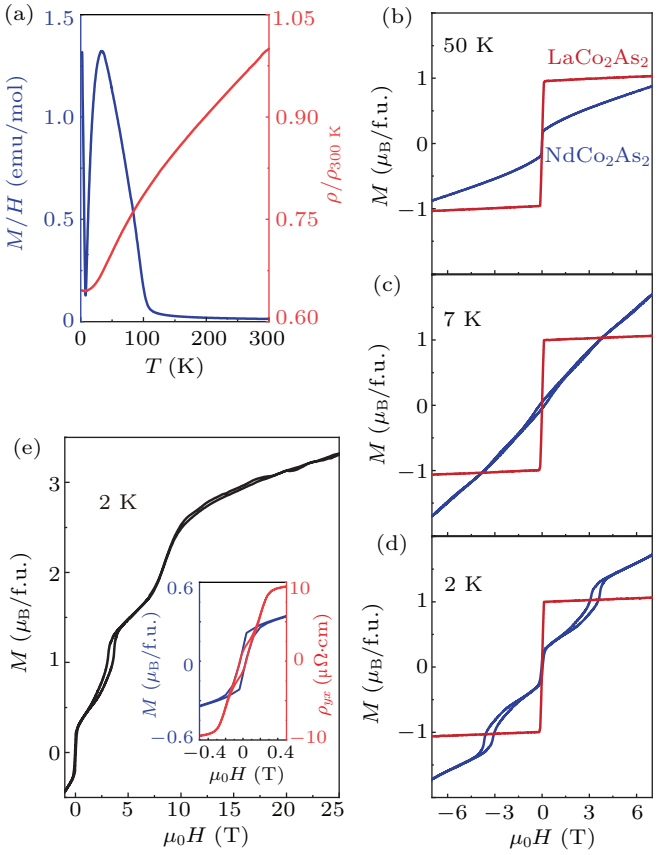


Fig. 2. Magnetic properties of $NdCo_2As_2$. (a) M/H (blue) in an external magnetic field of 0.1 T, and $\rho/\rho_{300\ K}$ in zero field. (b)–(d) Magnetic isothermal loops of $NdCo_2As_2$ (blue) and $LaCo_2As_2$ (red) in the applied field parallel to the direction of c axis at 50 K, 7 K, and 2 K, respectively. (e) High-field magnetization of $NdCo_2As_2$ at 2 K. Inset: M (blue) and ρ_{yx} (red) in low field at 2 K. Please note there are additional small hysteresis loops in $M(H)$ and $\rho_{yx}(H)$ at 2 K (inset in Fig. 2(e)), indicating a noncolinear magnetic texture in zero field at base temperature.

We comparably show the magnetic isothermal loops for FM $LaCo_2As_2$ and FIM $NdCo_2As_2$ at three representative temperatures: 50 K, 7 K, and 2 K, in Figs. 2(b)–2(d). The magnetic isotherms for $LaCo_2As_2$ have a typical profile of soft FM which has a coercive field less than 0.1 T and a nearly invariant M_{sat} 1.1 μ_B/f.u. As comparison, the $M(H)$ curve for $NdCo_2As_2$ at 50 K exhibits a spontaneous magnetization ($M_{0\,T}$) of 0.25 μ_B/f.u. and then gradually increases in the external field. This observation unveils that the FM Co sub-lattice in $NdCo_2As_2$ has much lower $M_{0\,T}$ than that in $LaCo_2As_2$. The gradual increase of $M(H)$ comes from a convergent effect of alignment of the Nd moments and polarization of the Co moments. When temperature decreases, the Nd moments grow up and cancel out the magnetization of Co moments, which results in a drop of the M_S in zero field. At 7 K, a small hysteresis loop is visible in low field. At 2 K, $M_{0\,T}$ turns back to the similar magnitude as at 50 K while an MMT occurs at 3 T.

We measured a piece of single-crystalline $NdCo_2As_2$ at 2 K in pulsed field in Wuhan National High Magnetic Field Laboratory in China and the result was shown in Fig. 2(e). Besides the MMT at 3 T, there is another MMT at 10 T and then the magnetization intends to saturate at higher field. The value of magnetization reaches 2.5 μ_B/f.u. at 10 T and then grows up to 3.2 μ_B/f.u. at 25 T which is still slightly less than the expected M_{sat} of the collinearly parallel Co moments 1 μ_B/2Co plus Nd moment of the Hund's rule ground state (3.2 μ_B/Nd^{3+}).

To shed a light on the magnetic structural changes in $NdCo_2As_2$, we demonstrate the $M(H)$ and its derivation to the field (dM/dH), $\rho_{yx}(H)$, and MR isothermals at representative temperatures in Fig. 3. To better describe the magnetic structural changes, we divide the temperatures below T_C into several regions in which the $M(H)$, $\rho_{yx}(H)$, and MR show different behaviors. An AHE is visible with a spontaneous Hall resistivity ($\rho_{yx,0\,T}$) below 80 K. From 80 K to about 30 K, $M_{0\,T}$ and $\rho_{yx,0\,T}$ gradually increase with decreasing temperature and there is no evident hysteresis loop. The MR remains negative in the whole field range above 50 K but starts to turn up in high field at 30 K. The negative MR, $M_{0\,T}$, and AHE with no visible hysteresis are similar as those in the FM state for $LaCo_2As_2$, but the magnitudes of $M_{0\,T}$, $\rho_{yx,0\,T}$, and MR are relatively smaller.

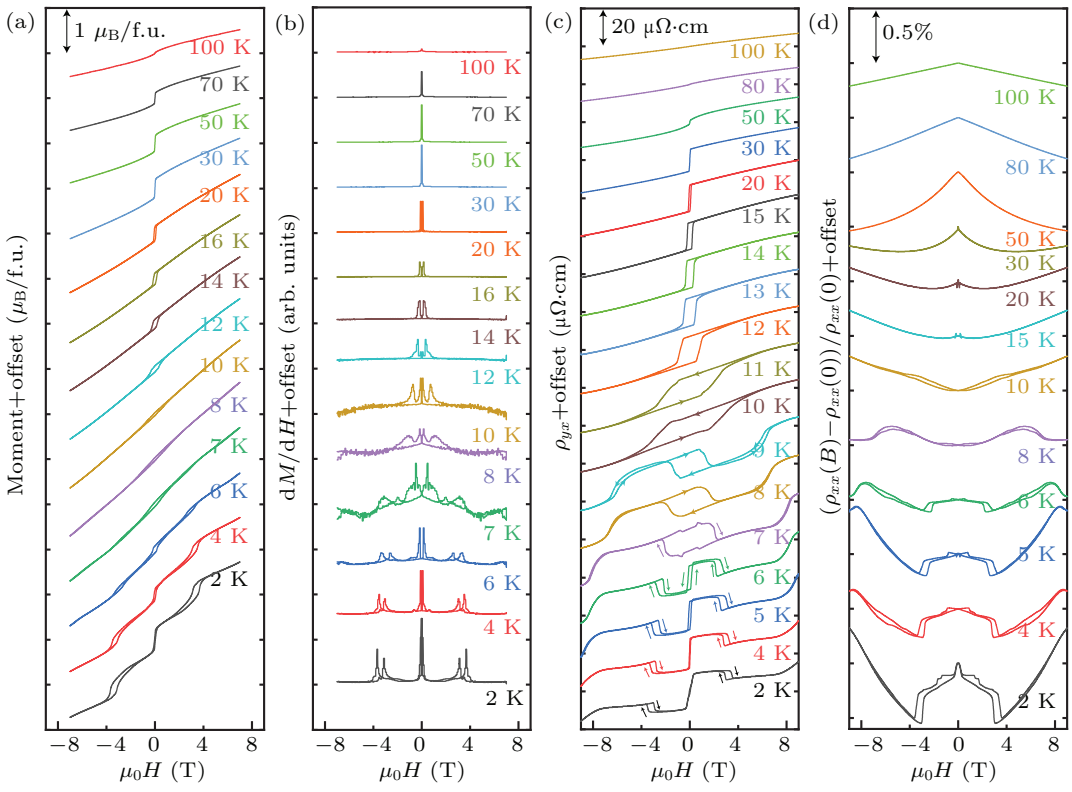


Fig. 3. Magnetic isothermals for $NdCo_2As_2$. (a) Magnetization, (b) derivative of the magnetization dM/dH, (c) Hall resistivities, and (d) MR at different temperatures in the applied field oriented parallel to the *c* axis. The current was applied along the *a* axis for transport measurements. The loops are shifted vertically upward with random offsets.

From 30 K to 10 K, pronounced hysteresis loops occur near zero field in $M(H)$ and $\rho_{yx}(H)$ isothermals. While the coercive fields of the hysteresis loops in $M(H)$ and $\rho_{yx}(H)$ grow up with decreasing temperature and become the greatest at 10 K, $M_{0\,T}$ continuously drops in this region. On the other hand, $\rho_{yx,0\,T}$ slightly increases from 30 K to 10 K. The MR curves change to positive and exhibit a butterfly-shaped feature near zero field due to the domain wall motion.[50]

Near T_{comp}, it is difficult to identify the hysteresis loop and MMT in $M(H)$ curves. However we can identify a series

of subtle magnetic structure changes by scrutinizing $\rho_{yx}(H)$ and MR curves. Striking and abrupt changes occur from 10 K to 9 K and then from 7 K to 6 K in $\rho_{yx}(H)$ curves. At 9 K, $\rho_{yx,0\ \mathrm{T}}$ changes the sign (please note the arrows which indicate the field sweeping direction), and then $\rho_{yx}(H)$ switches back at ± 7 T with the same amplitude as at zero field. The critical field of this MMT drifts to ± 10 T at 2 K which is visible in the $M(H)$ curve in Fig. 2(e), but near T_{comp} the corresponding change of magnetization is invisible.

The phenomenon of sign reversal in the $\rho_{yx,0\ \mathrm{T}}$ near T_{comp} is commonly observed in the R-TM alloy thin-films.[18,22–24] However for $NdCo_2As_2$ the reversed hysteresis loops of $\rho_{yx}(H)$ occur only in a very narrow temperature range from 9 K to 7 K. At 7 K a peculiar feature is visible at ± 1 T in the loop of $\rho_{yx}(H)$. At 6 K the loop collapses to an MMT at ± 3 T while $\rho_{yx,0\ \mathrm{T}}$ switches back to positive. From 6 K to 2 K the profiles of $\rho_{yx}(H)$ remain unchanged in principle. Yet a tiny loop of $\rho_{yx}(H)$ and $M(H)$ occurs near zero field at 2 K which is highlighted in the inset of Fig. 2(e).

Unlike the dramatic changes of $\rho_{yx}(H)$, $M(H)$ isothermals are almost identical from 10 K to 7 K. Below 7 K a pronounced $M_{0\ \mathrm{T}}$ reoccurs and an MMT occurs at about ± 3 T with large hysteresis. These features are more visible in the $\mathrm{d}M/\mathrm{d}H$ curves.

Below 10 K, the MR changes in a similar manner as the $\mathrm{d}M/\mathrm{d}H$ curves. Near T_{comp}, the weak butterfly-shaped features near zero field are almost identical. The MR curve shows a knee point at the MMT about ± 7 T and in higher field it changes to negative. At the other MMT about ± 3 T below 7 K, there is a pronounced jump of MR with large hysteresis.

To better demonstrate the magnetic compensation of $NdCo_2As_2$, we plot temperature dependence of the coercive field, $M_{0\ \mathrm{T}}$ and $\rho_{yx,0.5\ \mathrm{T}}$ below 20 K in Figs. 4(a) and 4(b). The coercive field of the loops in $\rho_{yx}(H)$ and $M(H)$ is maximum at 10 K while the M_{S} converges to zero. It is a general feature because the FIM requires a larger external magnetic field to obtain a sufficiently high Zeeman energy to switch the magnetization near T_{comp}.[23] On the other hand, $\rho_{yx,0.5\ \mathrm{T}}$ switches the sign when the temperature drops from 10 K to 9 K and then re-switches below 7 K. It is worth noting that the sign re-switch of the AHE has never been observed in R-TM FIM alloys. This indicates that $NdCo_2As_2$ undergoes an additional magnetic structure change rather than a simple magnetic pole reversal below T_{comp} as in R-TM alloys.[20,21]

We plot the temperature dependence of the values of $\rho_{yx}(H)$ in up and down sweeping fields in Figs. 4(c) and 4(d), respectively. When the magnetic field is less than 1 T, ρ_{yx} switches the sign from 10 K to 9 K and then re-switches from 7 K to 6 K. We notice the values of ρ_{yx} below 6 K fall into the same line as that above 10 K, which indicates similarity in the magnetic structures. The sign re-switch vanishes in 3 T of up sweeping field and 2 T of down sweeping field, corresponding to the MMT at ± 3 T with large hysteresis. In higher field the value of ρ_{yx} at base temperature increases with the field. The two MMTs and the re-switch of ρ_{yx} indicate that $NdCo_2As_2$ has at least three different magnetic structures in various temperatures and fields.

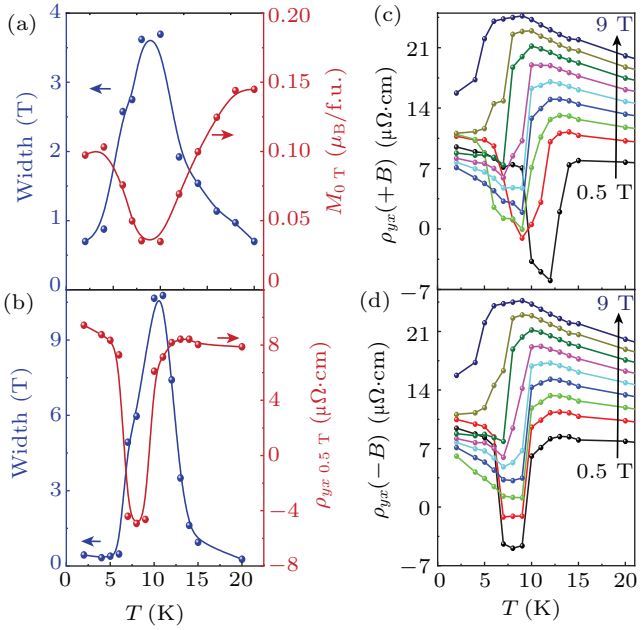


Fig. 4. Signature of the compensation point in $NdCo_2As_2$. (a) and (b) Temperature dependence of the width and the magnitude of the loops in $M(H)$ and $\rho_{yx}(H)$ near zero field, respectively. (c) and (d) Temperature dependence of the ρ_{yx} in different magnetic fields when the field sweeps up (+) and down (−), respectively.

4. Analysis and discussion

Now we analyze the AHE in $LaCo_2As_2$ and $NdCo_2As_2$ and clarify their mechanisms, for the sake of understanding their magnetic structures. For a spontaneous Hall effect, AHC (σ_{AH}) is obtained from the relation

$$\sigma_{\mathrm{AH}} \approx \rho_{yx}^{\mathrm{AH}}/\rho_{xx}^{2},$$

where ρ_{xx} represents the longitudinal resistivity in zero field. Figure 5(a) shows that ρ_{yx}^{AH} for $LaCo_2As_2$ reaches its maximum at about 100 K, while σ_{AH} gradually increases with decreasing temperature. Realizing $M_{0\ \mathrm{T}}$ changes from 0.6 μ_{B}/f.u. to 1.1 μ_{B}/f.u. from 150 K to 2 K, we take $M(T)$ into account to disentangle the AHE into intrinsic and extrinsic parts.[51–55] As the intrinsic part of AHC is independent of the life time of electrons while the extrinsic part is proportional to the life time, the plot of $\rho_{yx}^{\mathrm{AH}}/M(T)\rho_{xx}$ with repect to ρ_{xx} will fall into a linear relation in which the slope is the intrinsic contribution while the intercept is the extrinsic contribution if the mechanism of AHE does not change in temperatures.[56–59] As shown in Fig. 5(c), the linear scaling with a zero intercept reveals that the mechanism is purely intrinsic.

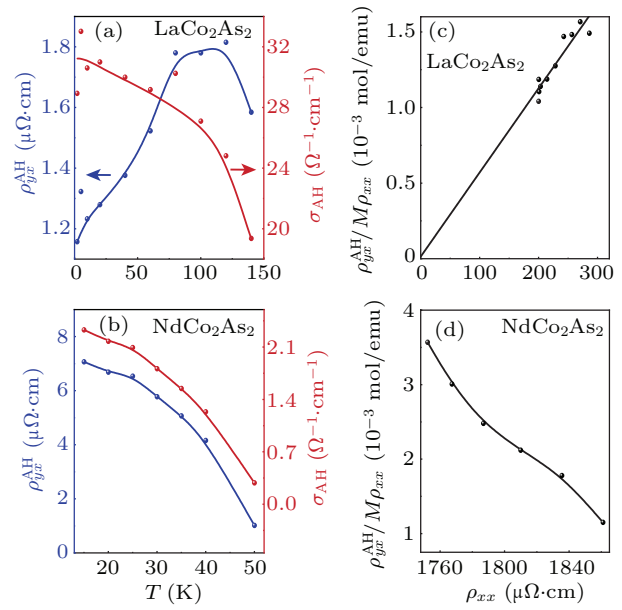


Fig. 5. Spontaneous Hall effect in $LaCo_2As_2$ and $NdCo_2As_2$. (a) and (b) Temperature dependence of the spontaneous Hall resistivity ρ_{yx}^{AH} and conductivity σ_{AH} for $LaCo_2As_2$ and $NdCo_2As_2$, respectively. (c) Scaling of ρ_{yx}^{AH} indicates an intrinsic mechanism of AHE in $LaCo_2As_2$. (d) Scaling of ρ_{yx}^{AH} is invalid for $NdCo_2As_2$, indicating complex origination.

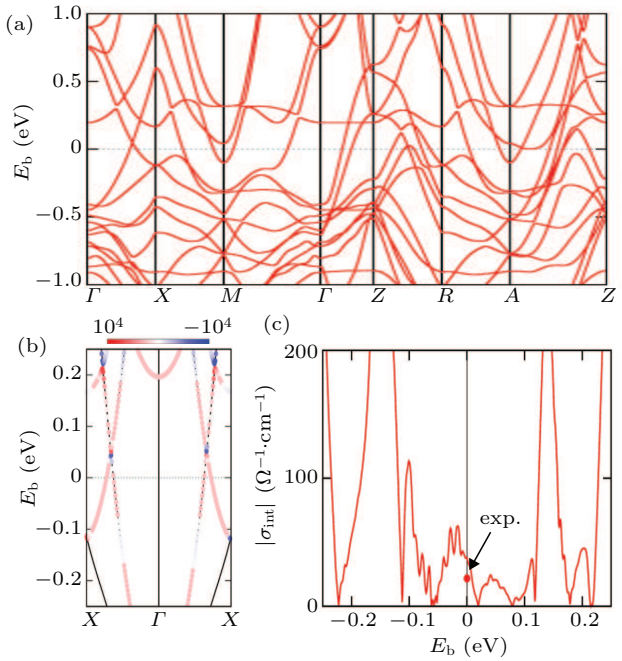


Fig. 6. Berry curvature distribution and AHC of $LaCo_2As_2$. (a) Renormalized DFT band structures. (b) Renormalized DFT band structure with Berry curvature distribution along X–Γ–X. (c) Intrinsic part of AHC.

To clarify the relationship between the AHE and Berry curvature field in $LaCo_2As_2$, we preformed first principle calculations to compute the electronic structure and topological property. The renormalized DFT band structure of $LaCo_2As_2$ in the FM state is shown in Fig. 6, which is in good agreement with the ARPES results.[38] The bands mainly from Co-3d contribution intersect with each other and form nodes around the Fermi level. Due to the large Fermi velocity of the d-electron bands, the corresponding Berry curvature is small, and the positive and negative contributions of them mostly offset each other. The low Berry curvature density results in low AHE, as shown in Fig. 6(c), which can naturally explain the intrinsic AHE of the experimental results.

We now try to understand the spontanous Hall effect of $NdCo_2As_2$ in the temperature range from 10 K to 50 K. As shown in Fig. 5(b), both ρ_{yx}^{AH} and σ_{AH} are strongly enhanced when temperature drops. We notice that the $\rho_{xx}(T)$ changes less than 10% from 50 K to 10 K whereas $M_{0\ T}$ changes from 0.20 μ_B/f.u. at 50 K to the maximum value of 0.24 μ_B/f.u. at 33 K and then to a very small value of 0.03 μ_B/f.u. at 7 K. Obviously, the change of σ_{AH} and ρ_{yx}^{AH} has no explicit functional relation with the change of $\rho_{xx}(T)$ or magnetization either. The failure of the scaling law for $NdCo_2As_2$ is confirmed in Fig. 5(d), which indicates that the AHE is not determined by M_S of the anti-parallel Co and Nd sub-lattices.

The sign switch of the spontanous Hall effect near T_{comp} in $NdCo_2As_2$ indicates that the AHE is stemming from the Co sub-lattice although the electronic structure and Berry curvature field will be different from that of $LaCo_2As_2$. Because the AHE is extremely sensitive to the magnetic structure change, we can infer the nature of the magnetic compensation and MMTs and build up a phase diagram for $NdCo_2As_2$, similar to the R-TM alloys.[18,23–25]

In order to better demonstrate the change of ρ_{yx} in the MMTs, we subtract the value at 15 K as the linear background ($\Delta\rho_{yx} = \rho_{yx} - \rho_{yx,15\ K}$). The contour maps in the plane of temperature and magnetic field are shown in Figs. 7(a) and 7(b) in which the field swept up and down, respectively. It is noteworthy that the value of $\Delta\rho_{yx}$ at low temperature in zero field is close to that at high temperature and field, which indicates that the magnetizations of the Co sub-lattice are same in the two regions. The sign reversal of the AHE occurs in the middle region in which the direction of the Co magnetization is anti-parallel to the external field.

Such complicated magnetic structural changes are not anticipated in the R-TM alloys which typically go through only one spin-flop transition in H_{sf}.[20,21] In the R-TM alloys, the anti-parallel magnetic moments of R and TM get canted and form a noncollinear structure in a magnetic field. After going through the spin-flop transition, the canting angle is further controlled by the increasing magnetic field higher than H_{sf} until both moments align collinearly along the strong saturation field. However in RCo_2As_2 the relatively weak RKKY interaction between the local moments of R^{3+} ions may give rise to an AFM ordering of the R sub-lattice. We compare the magnetic structural changes of $PrCo_2As_2$ which have been identified by the neutron diffraction experiment.[35] While the T_C for the Co sub-lattice is 140 K, the Pr moments start to order at 25 K, anti-parallel to the Co moments. At base temperature the Pr atoms form two sets of nonequivalent magnetic sub-lattices

in zero external field due to the magnetic interaction between the Pr moments. We believe similar magnetic structure exists in $NdCo_2As_2$ at base temperature. Noticing that $M_{0\ \mathrm{T}}$ and ρ_{yx}^{AH} at 2 K are identical to that above 10 K, we infer that the Nd sub-lattice forms an AFM texture while the Co sub-lattice aligns FM and contributes $M_{0\ \mathrm{T}}$ and ρ_{yx}^{AH} solely in region I in the phase diagram (Fig. 7(c)). Magnetization of Nd moments no longer cancel out that of Co moments, resulting in a sharp increase of $M(T)$ curve at low temperature in Fig. 2(a). The MMT at ± 3 T corresponds to a spin flop transition in which half of the Nd moments switch the direction along with the external field, which leads to a reversal of the magnetization of the Co sub-lattice. The second MMT at high field is a spin-flop transition (H_{sf}) above which the magnetization of the Co sub-lattice re-switches, similar as the R-TM alloys.[20,21]

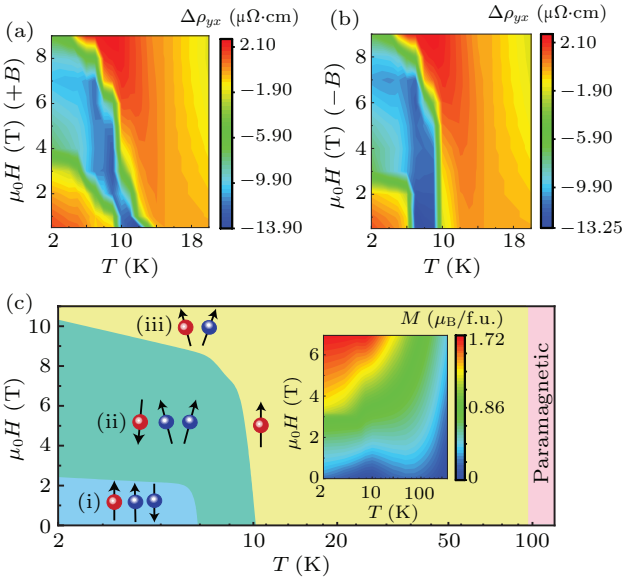


Fig. 7. (a) and (b) Contour maps in the plane of temperature and magnetic field for Hall resistivities in $NdCo_2As_2$ with (a) up and (b) down field sweep. The color bars at the side of the maps represent the Hall resistivities after subtracting the value at 15 K, $\Delta\rho_{yx} = \rho_{yx} - \rho_{yx,15\ \mathrm{K}}$. (c) Phase diagram of $NdCo_2As_2$. Arrows visualize the orientations of Co (red) and Nd moments (blue). The inset shows the contour map in the plane of temperature and magnetic field for the magnitude of magnetization.

The observed change of MR in the MMTs can be interpreted by the inferred magnetic phase diagram. At low temperature, the MMT in low field is assigned to the reverse of half of large Nd-4f-electron moments, which causes significant changes in the M_{S} and electron scattering. Correspondingly, we observed a dramatic change with large hysteresis in the $M(H)$ and MR curves. As comparisons, the MMT at high field is only assigned to the reverse of small Co-d-electron moments, resulting in a much smaller change in electron scattering. In the above discussion we ignore the small hysteresis loops in $M(H)$ and $\rho_{yx}(H)$ at 2 K (inset in Fig. 2(e)), which indicates an additional noncolinear magnetic texture in zero field at base temperature. Future studies, such as neutron diffraction, will help to unveil the details of the magnetic structures in $NdCo_2As_2$.

5. Conclusion

In summary, we have studied the magnetic and transport properties in response to the complex magnetic structures of FIM $NdCo_2As_2$ and FM $LaCo_2As_2$ as comparisons. Unlike the purely intrinsic mechanism in $LaCo_2As_2$, the AHE in $NdCo_2As_2$ is sensitive to the multiple phase transitions induced by the competing interaction between Nd an Co sub-lattices especially near the magnetic compensation point. Understanding the relationship between the magnetic structural change and AHE will help to explore the complicated phase diagram of FIM compounds, which may lead to a promising platform for future spintronic devices with higher speed and density.

Acknowledgements

The authors thank Jia Li, Wei Han for the fruitful discussions. Project supported by the National Key Research and Development Program of China (Grant No. 2018YFB1502502), the National Natural Science Foundation of China (Grant Nos. 12141002 and 12225401), the Fund from Foshan Xianhu Laboratory of the Advanced Energy Science and Technology Guangdong Laboratory. The work in the high magnetic field lad was supported by the Interdisciplinary Program of Wuhan National High Magnetic Field Center (Grant No. WHMFC202123), Huazhong University of Science and Technology. Z. Y. was supported by the National Natural Science Foundation of China (Grant Nos. 12074041 and 11674030), the Foundation of the National Key Laboratory of Shock Wave and Detonation Physics (Grant No. 6142A03191005), the National Key Research and Development Program of China (Grant No. 2016YFA0302300), and the startup funding of Beijing Normal University. The calculations were carried out with high performance computing clusters of Beijing Normal University in Zhuhai.

References

[1] Nagaosa N, Sinova J, Onoda S, MacDonald A H and Ong N P 2010 *Rev. Mod. Phys.* **82** 1539
[2] Karplus R and Luttinger J M 1954 *Phys. Rev.* **95** 1154
[3] Smit J 1955 *Physica* **21** 877
[4] Smit J 1958 *Physica* **24** 39
[5] Berger L 1970 *Phys. Rev. B* **2** 4559
[6] Xiao D, Chang M C and Niu Q 2010 *Rev. Mod. Phys.* **82** 1959
[7] Nakatsuji S, Kiyohara N and Higo T 2015 *Nature* **527** 212
[8] Nayak A K, Fischer J E, Sun Y, Yan B, Karel J, Komarek A C, Shekhar C, Kumar N, Schnelle W, Kübler J, Felser C and Parkin S S 2016 *Sci. Adv.* **2** e1501870
[9] Smejkal L, MacDonald A H, Sinova J, Nakatsuji S and Jungwirth T 2022 *Nat. Rev. Mater.* **7** 482
[10] Néel L 1948 *Ann. Phys.* (Paris) **3** 137
[11] Pauthenet R 1958 *J. Appl. Phys.* **29** 253
[12] Clark A E and Callen E 1968 *J. Appl. Phys.* **39** 5972
[13] McGuire T R, Gambino R J and Taylor R C 1977 *J. Appl. Phys.* **48** 2965
[14] Malmhäll R 1983 *J. Appl. Phys.* **54** 5128

[15] Stanciu C D, Kimel A V, Hansteen F, Tsukamoto A, Itoh A, Kirilyuk A and Rasing T 2006 *Phys. Rev. B* **73** 220402

[16] Finley J and Liu L 2016 *Phys. Rev. Appl.* **6** 054001

[17] Mishra R, Yu J, Qiu X, Motapothula M, Venkatesan T and Yang H 2017 *Phys. Rev. Lett.* **118** 167201

[18] Kim K J, Kim S K, Hirata Y, Oh S H, Tono T, Kim D H, Okuno T, Ham W S, Kim S, Go G, Tserkovnyak Y, Tsukamoto A, Moriyama T, Lee K and Ono T 2017 *Nat. Mater.* **16** 1187

[19] Jungwirth T, Marti X, Wadley P and Wunderlich J 2016 *Nat. Nanotechnol.* **11** 231

[20] Becker J, Tsukamoto A, Kirilyuk A, Maan J C, Rasing T, Christianen P C M and Kimel A V 2017 *Phys. Rev. Lett.* **118** 117203

[21] Bhatt R C, Ye L X, Hai N T, Wu J C and Wu T H 2021 *J. Magn. Magn. Mater.* **537** 168196

[22] Okuno T, Kim K J, Tono T, Kim S, Moriyama T, Yoshikawa H, Tsukamoto A and Ono T 2016 *Appl. Phys. Express* **9** 073001

[23] Xu Y, Chen D, Tong S, Chen H, Qiu X, Wei D and Zhao J 2020 *Phys. Rev. Appl.* **14** 034064

[24] Davydova M D, Skirdkov P N, Zvezdin K A, Wu J C, Ciou S Z, Chiou Y R, Ye L X, Wu T H, Bhatt R C, Kimel A V and Zvezdin A K 2020 *Phys. Rev. Appl.* **13** 034053

[25] Park J, Hirata Y, Kang J H, Lee S, Kim S, Van Phuoc C, Jeong J R, Park J, Park S Y, Jo Y, Tsukamoto A, Ono T, Kim S K and Kim K J 2021 *Phys. Rev. B* **103** 014421

[26] Shi W, Muechler L, Manna K, Zhang Y, Koepernik K, Car R, van den B J, Felser C and Sun Y 2018 *Phys. Rev. B* **97** 060406

[27] Park M, Han G and Rhim S H 2022 *Phys. Rev. Res.* **4** 013215

[28] Yin J X, Ma W, Cochran T A, *et al.* 2020 *Nature* **583** 533

[29] Ma W, Xu X, Yin J X, Yang H, Zhou H, Cheng Z J, Huang Y, Qu Z, Wang F, Hasan M Z and Jia S 2021 *Phys. Rev. Lett.* **126** 246602

[30] Marchand R and Jeitschko W 1978 *J. Solid State Chem.* **24** 351

[31] Jia S, Jiramongkolchai P, Suchomel M R, Toby B H, Checkelsky J G, Ong N P and Cava R J 2011 *Nat. Phys.* **7** 207

[32] Lai Y, Chan J Y and Baumbach R E 2022 *Sci. Adv.* **8** eabp8264

[33] Tan X, Tener Z P and Shatruk M 2018 *Acc. Chem. Res.* **51** 230

[34] Thompson C M, Tan X, Kovnir K, Garlea V O, Gippius A A, Yaroslavtsev A A, Menushenkov A P, Chernikov R V, Büttgen N, Krätschmer W, Zubavichus Y V and Shatruk M 2014 *Chem. Mater.* **26** 3825

[35] Tan X 2016 *Synthesis and Investigation of Ternary Intermetallics as Itinerant Magnets*, Ph. D. Dissertation (The Florida State University)

[36] Thompson C M 2012 *Magneto-Structural Correlations in Rare Earth-Cobalt Pnictides*, Ph. D. Dissertation (The Florida State University)

[37] Menushenkov A P, Yaroslavtsev A A, Geondzhian A Y, Chernikov R V, Zubavichus Y V, Tan X and Shatruk M 2015 *J. Supercond. Nov. Magn.* **28** 995

[38] Cheng Z J, Huang Y, Zheng P, *et al.* 2023 arXiv preprint arXiv: 2302.12113

[39] Thompson C M, Kovnir K, Eveland S, Herring M J and Shatruk M 2011 *Chem. Commun.* **47** 5563

[40] Kresse G and Furthmüller J 1996 *Comp. Mater. Sci.* **6** 15

[41] Pizzi G, Vitale V, Arita R, *et al.* 2020 *J. Phys.: Condens. Matter* **32** 165902

[42] Wu Q, Zhang S, Song H F, Troyer M and Soluyanov A A 2018 *Comput. Phys. Commun.* **224** 405

[43] Haule K, Yee C H and Kim K 2010 *Phys. Rev. B* **81** 195107

[44] Kotliar G, Savrasov S Y, Haule K, Oudovenko V S, Parcollet O and Marianetti C A 2006 *Rev. Mod. Phys.* **78** 865

[45] Blaha P, Schwarz K, Madsen G K, Kvasnicka D and Luitz J 2001 *An augmented plane wave+local orbitals program for calculating crystal properties* **60** 1

[46] Mao H and Yin Z 2018 *Phys. Rev. B* **98** 115128

[47] Haule K 2015 *Phys. Rev. Lett.* **115** 196403

[48] Haule K 2007 *Phys. Rev. B* **75** 155113

[49] Werner P, Comanac A, De'Medici L, Troyer M and Millis A J 2006 *Phys. Rev. Lett.* **97** 076405

[50] Marrows C H and Dalton B C 2004 *Phys. Rev. Lett.* **92** 097206

[51] Zeng C, Yao Y, Niu Q and Weitering H H 2006 *Phys. Rev. Lett.* **96** 037204

[52] Zhu T 2014 *Chin. Phys. B* **23** 047504

[53] Ding J J, Wu S B, Yang X F and Zhu T 2015 *Chin. Phys. B* **24** 027201

[54] Zhu L J, Nie S H and Zhao J H 2016 *Phys. Rev. B* **93** 195112

[55] Hazra B K, Kaul S N, Srinath S, Raja M M, Rawat R and Lakhani A 2017 *Phys. Rev. B* **96** 184434

[56] Hou D, Su G, Tian Y, Jin X, Yang S A and Niu Q 2015 *Phys. Rev. Lett.* **114** 217203

[57] Yue D and Jin X 2017 *J. Phys. Soc. Jpn.* **86** 011006

[58] Wang G, Sun Z, Si X and Jia S 2020 *Chin. Phys. B* **29** 077503

[59] Zhou H, Chang G, Wang G, Gui X, Xu X, Yin J X, Guguchia Z, Zhang S S, Chang T R, Lin H, Xie W, Hasan M Z and Jia S 2020 *Phys. Rev. B* **101** 125121